JOURNAL OF AIRCRAFT
Vol. 42, No. 3, May–June 2005

Control Surface Response of a Blended Wing Body Aeroelastic Wind-Tunnel Model

Martin Carlsson*
Royal Institute of Technology, SE-100 44 Stockholm, Sweden

The aeroelastic behavior of a blended wing body- (BWB-) type wind-tunnel model is investigated. The design concept, numerical modeling, and experimental procedures are described together with comparisons of numerical and experimental results. The main focus is on aeroelastic response due to static and dynamic control surface deflections. The numerical analysis is performed using a finite element structural model and doublet lattice aerodynamics. The agreement between the predicted and experimental aerodynamic loads and aeroelastic deformations are good overall. However, the investigation shows that the loads due to control surface deflections are slightly overpredicted by the numerical analysis. The results indicate that available numerical methods are capable of predicting aeroelastic behavior of the BWB-type aircraft with reasonable accuracy.

Introduction

TODAY, composite materials in combination with numerical optimization methods are sometimes used for design of efficient aircraft structures. Very flexible so-called active aeroelastic structures (e.g., Schweiger and Krammer[1]) are investigated, which enables the possibility to control the deformation of the structure and to make use of the elastic behavior to further improve the overall performance of the aircraft. However, very lightweight and flexible structures can, if not designed carefully, suffer from performance degradation. Phenomena such as wing divergence, flutter, reduced wing efficiency, and control reversal have to be accounted for in the design process. Often, some of the objectives conflict with each other, and therefore, a carefully balanced design procedure is required.[2]

Methods for optimization taking aeroelastic effects into account are presented by, for example, Bowman et al.[3] and Mantegazza and Ricci.[4] However, it has been shown that numerical optimization can lead to numerically feasible designs that are extremely sensitive to uncertainties in the numerical model.[5] Robust analysis and design that consider uncertainties in the numerical models are areas where a lot of effort is being concentrated today, for example, by Lind and Brenner[6] and Borglund.[7]

Aeroelastic experiments are of vital importance to verify if the numerical methods are useful in practice or not. Aeroelastic wind-tunnel models have been used for many years for verification purposes and for estimating uncertainties in numerical representations, as by Schneider et al.,[8] Sensburg et al.,[9] and Dafnis et al.[10] As presented by Amiryants and Ishmuratov,[11] the possibility to replace individual parts of the elastic models to change the stiffness and mass distributions is often desired. Such models are typically very expensive due to the complex design and the high accuracy required in the manufacturing.

The particular wind tunnel model considered in this paper is designed for low-speed aeroelastic investigations of a blended wing body (BWB) transport aircraft. A simplified model design concept is utilized. However, the model has much of the desired functionality, such as the possibility to change stiffness and mass distributions. Also, the model enables the possibility to add new functionality, such as the control surfaces used in this investigation. Whereas the design and initial validation of the model are presented in Ref. 12, the focus of this paper is the continued work including effects of static and dynamic control surface deflections.

The work has been carried out within the project Multi-Disciplinary Design and Optimisation for Blended Wing Body Configuration (MOB). Much work has also been carried out in various other projects to investigate the potential advantages of the BWB concept. The BWB concept, in general, is described by Liebeck et al.,[13] whereas control system issues are treated by, for example, Cameron and Princen.[14]

Wind-Tunnel Model

The wind-tunnel model used in this study is a semispan model of a BWB aircraft. The geometry is not an exact representation of an existing BWB configuration but is chosen to represent a typical aircraft of the BWB type. The geometry of the model is shown in Fig. 1. Only the outer part of the model is elastic, whereas the inner part, representing the fuselage, is rigid. The elastic part of the model is designed using the segmented approach.[15] With this concept, the stiffness of the wing is determined entirely by an internal wing beam. In this case, the beam is made from a carbon fiber/epoxy composite.[12] Because no representative stiffness distribution data from a BWB aircraft were available at the time of model design, the stiffness distribution of the wing resembles the stiffness of a conventional transport aircraft. Further, the stiffness of the model is scaled to match the low-speed conditions at which the testing is performed.

The outer geometry of the model is achieved using eight rigid wing sections clamped to the beam in a way that allows them to move individually without affecting the stiffness of the wing. The wing sections can easily be replaced, and in this study, wing sections 6 and 7 are equipped with 20% chord trailing-edge control surfaces (Fig. 1). Computer-controlled electrical servos are used to actuate the control surfaces. Although they can be controlled separately, they are only used as one single control surface in this study. Figure 2 is a photograph of the two control surfaces. A six-component internal balance is mounted inside the fuselage to measure the loads acting on the elastic part of the model. Further details about the model may be found in Ref. 12.

Numerical Model

The numerical representation of the wind tunnel model considered in this study is developed using MSC/NASTRAN.[16] The structural modeling is rather simple because the wing beam is the only elastic member. The beam is modeled using eight-node shell elements with anisotropic material properties. The beam properties in terms of thickness and composite layup vary from the root to the tip

Presented as Paper 2003-450 at the 41st Aerospace Sciences Meeting and Exhibit, Reno, NV, 6–9 January 2003; received 26 September 2003; accepted for publication 13 November 2003.

*Ph.D. Student, Department of Aeronautical and Vehicle Engineering, Teknikringen 8. Member AIAA.

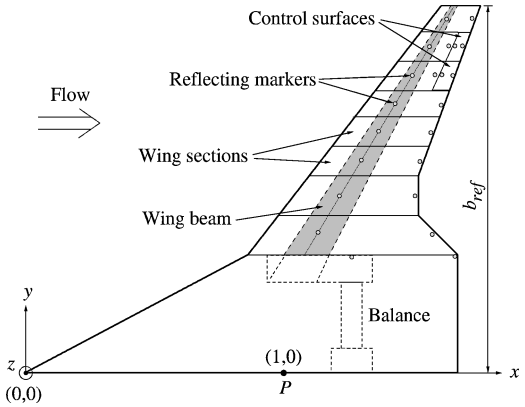

Fig. 1 Wind-tunnel model.

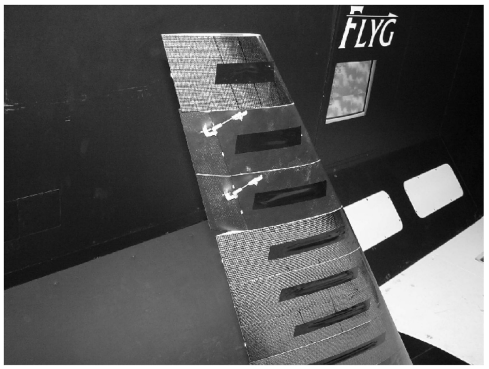

Fig. 2 Control surfaces.

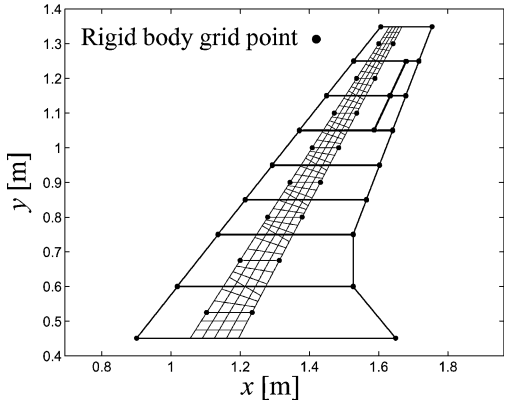

Fig. 3 Structural model of the elastic part.

to achieve the desired elastic properties. Therefore, the numerical model of the beam is divided into regions with piecewise constant material properties. Convergence studies, with respect to the beam eigenfrequencies, were performed to determine the required mesh density. It was concluded that 192 elements (4 chordwise × 48 spanwise) were sufficient to represent the wing beam.

The stiff wing sections are structurally modeled as rigid bodies connected to the beam at the points of physical attachment. Also the control surfaces are modeled as rigid bodies. For the static analysis, the control surface rigid bodies are fixed to the motion of their corresponding wing section. For the dynamic response analysis, the relative motion of the control surfaces are constrained to the motion of their corresponding wing section using the multipoint constraint method.[16]

The mass properties of the wing sections are experimentally measured and numerically represented by attaching masses with rotational mass moment of inertia to the beam. Because the control surfaces are very light, their mass moment of inertia are neglected in the analysis. Figure 3 shows the numerical model of the outer

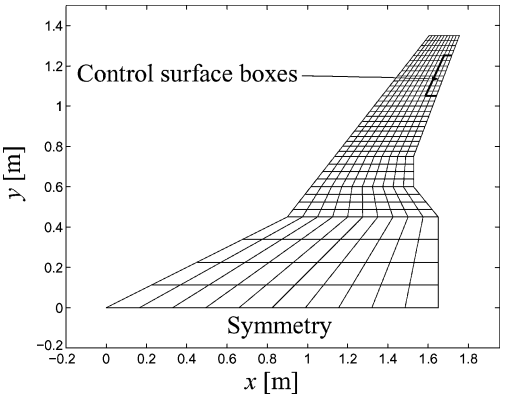

Fig. 4 Aerodynamic mesh.

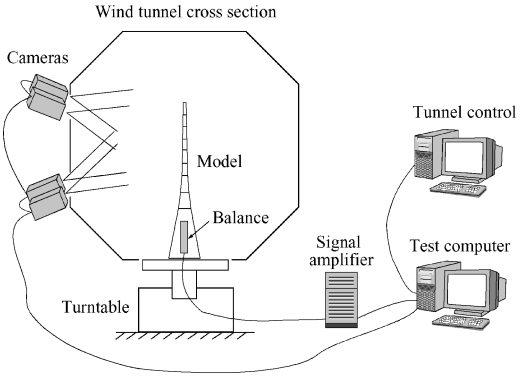

Fig. 5 Experimental setup.

part of the elastic model, including the wing beam, wing sections, and control surfaces.

The aerodynamic loads are modeled using the doublet lattice method.[17] Each stiff wing section is modeled as one separate panel containing 10 chordwise and 4 spanwise aerodynamic boxes. The aerodynamic boxes of each panel are coupled to the motion of the corresponding rigid body representing the wing section using spline functions. The aerodynamic boxes representing the control surfaces are coupled to the corresponding grid points representing the control surface rigid bodies. The aerodynamic mesh is shown in Fig. 4.

Also the fuselage is represented by one panel containing 10×4 aerodynamic boxes. The fuselage panel is, however, not coupled to the structure because the aim is to compare loads from the outer elastic part of the model only. Furthermore, the aerodynamic model is symmetric around the model centerline to account for the wind-tunnel boundary.

Experimental Setup

The experimental testing was performed in the low-speed wind tunnel L2000 at the Royal Institute of Technology (Kungliga Tekniska Högskolan), Stockholm. The environmental test conditions were room temperature and atmospheric pressure throughout the tests. Standard atmosphere at sea level conditions was used in all conversions between dynamic pressure q and airspeed u.

Aerodynamic loads acting on the elastic part of the model are measured using the balance mounted in the rigid fuselage. The elastic deformations and control surface deflections are measured using an optical positioning system mounted in the wind tunnel.[18] For this purpose, passive reflecting markers are attached to the model according to Fig. 1. The optical system is further described in Ref. 19.

For dynamic measurements, it is of vital importance to measure the aerodynamic loads and the elastic deformations simultaneously. For this purpose, the cameras are here used with an external trigger option, which permits the measurement of the deformation of the model at the same instant that the voltages of the internal balance are measured. A schematic layout of the experimental setup is shown in Fig. 5. The test program is implemented in LabView,[20] which

controls the dynamic pressure in the wind tunnel and the position of the turntable where the model is mounted and also the control surface deflection according to a predefined test schedule. Most important, all data acquisition is performed simultaneously.

For the static measurements, the positions of the markers and the balance voltages are sampled at 10 Hz for 3 s for each test condition, dynamic pressure, angle of attack, and control surface deflection. The wing deformations and aerodynamic loads are calculated from the mean values of all samples. For the dynamic testing, both wing deformations and balance voltages are sampled simultaneously at 100 Hz.

Results

The structural part of the numerical model was validated using vibration testing as reported in Ref. 12. Before this study, two of the wing sections were replaced with two corresponding wing sections including control surfaces. The mass properties of the new sections were experimentally measured, and the numerical model was updated with the new mass data.

The numerically predicted and experimentally measured eigenfrequencies for the model including control surfaces are shown in Table 1. The largest deviation between experimentally measured and predicted frequencies is observed for modes 3 and 6, which are both dominated by torsional deformation. Similar observations were made in the previous study,[12] in which was concluded that the torsional stiffness of the model was slightly higher than predicted. However, no update of the numerical model was performed because the overall agreement was satisfactory.

A flutter analysis is performed to estimate a boundary for the experimental testing with respect to flutter instability. The analysis is performed using a modal formulation including the first seven eigenmodes. The nonlinear eigenvalue problem associated with the flutter analysis is solved using the p–k method.[16] The root-locus plot of the three leading eigenvalues is shown in Fig. 6. Each mode is tracked from $u = 10$ m/s (marked by ○) to the critical speed (marked by ×). At $u = 59$ m/s, the wing is predicted to suffer from a 20-Hz flutter instability caused by eigenvalue B. The divergence speed of the model is predicted to be over 100 m/s. With respect to this analysis, the maximum airspeed for the wind-tunnel testing was limited to 40 m/s, to have a rather high safety margin to the flutter boundary.

Table 1 Predicted and experimentally measured eigenfrequencies

Mode	f_{pred}, Hz	f_{exp}, Hz	$\lvert(f_{\text{exp}} - f_{\text{pred}})/f_{\text{exp}}\rvert$, %
1	5.47	5.50	0.5
2	22.3	21.4	4.2
3	33.4	36.5	8.5
4	52.6	52.6	0.0
5	60.0	64.0	6.3
6	69.7	74.5	6.4
7	96.1	93.4	2.9

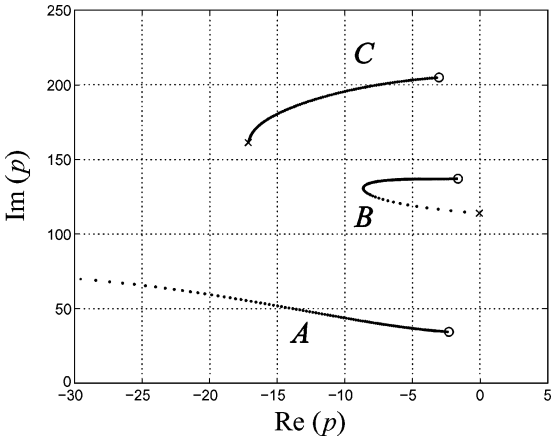

Fig. 6 Root-locus plot of the three leading eigenvalues.

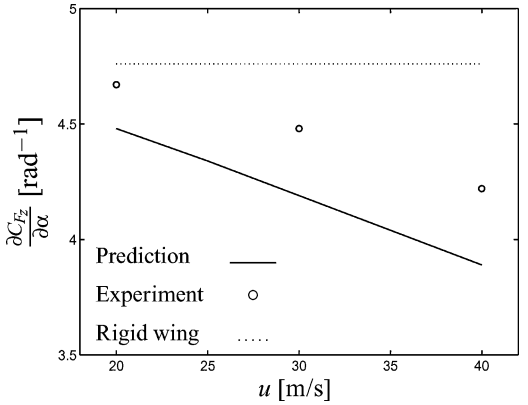

Fig. 7 Derivative of C_{F_z} with respect to α as a function of airspeed.

Aeroelastic Wing Efficiency

A comparison of predicted and experimentally measured aerodynamic loads as function of angle of attack is presented in Ref. 12. Overall, the agreement is very good, although the experimentally measured loads are about 7% larger than predicted. One possible reason for this is that the torsional stiffness of the model is slightly higher than what the numerical model predicts. This conclusion is also verified by studying the aeroelastic deformations for various flight conditions. The local angle of attack is decreased toward the tip of the wing, but not as much as numerically predicted.

The aerodynamic derivative of C_{F_z} with respect to the angle of attack α as a function of airspeed u is presented in Fig. 7. Here, C_{F_z} represents the normalized coefficient of the force F_z in the z direction (body-fixed system) according to

$$C_{F_z} = F_z/q S_{\text{ref}} \tag{1}$$

where q is the dynamic pressure and $S_{\text{ref}} = 0.325$ m^2 is the reference area. In Fig. 7, the numerical prediction including elastic effects is presented together with experimental results. The numerical prediction for a rigid model is also shown. To quantify the elastic effects, the aeroelastic wing efficiency E_w can be considered according to

$$E_w = \left[\frac{\partial C_{F_z}}{\partial \alpha}\right]_{\text{elastic}} \Bigg/ \left[\frac{\partial C_{F_z}}{\partial \alpha}\right]_{\text{rigid}} \tag{2}$$

Here, E_w decreases with increasing airspeed just as predicted by the numerical model. This behavior is expected for an aft-swept wing if the structure is not especially tailored for another aeroelastic behavior. The experimental results show that the tendency is the same as predicted, although the efficiency of the wing is somewhat higher within the tested airspeed range. At low speed (20 m/s), the aeroelastic effects are more or less negligible, but as the airspeed increases, the effect becomes significant. At 40 m/s, the wing efficiency is reduced by approximately 10%.

Static Control Surface Response

The static response due to control surface deflection is studied for deflection angles from −15 to 15 deg. The moment M_x around the x axis as a function of control surface deflection at three different airspeeds is presented in Fig. 8.

The measured moments seems to be fairly linear with respect to control surface deflection within the tested envelope. At $u = 20$ m/s, the experimental moment to the magnitude is 15% smaller than predicted. At $u = 30$ m/s, predicted and measured moments agree within 8%. The slope of the curve is somewhat higher than for the lower airspeed. When the airspeed is increased to 40 m/s, the numerical model predicts the slope of the curve to be reduced. This behavior is also experienced in the experiment, although the measured loads (to the magnitude) are slightly larger than predicted.

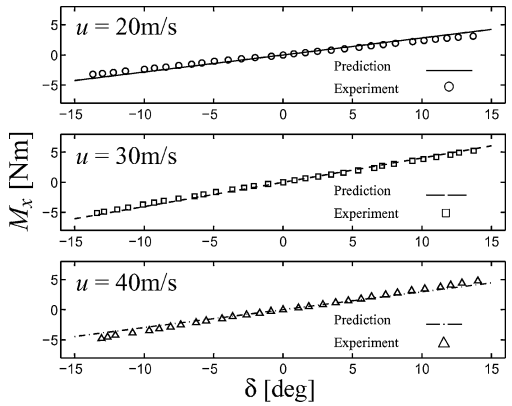

Fig. 8 Rolling moment M_x as a function of control surface deflection.

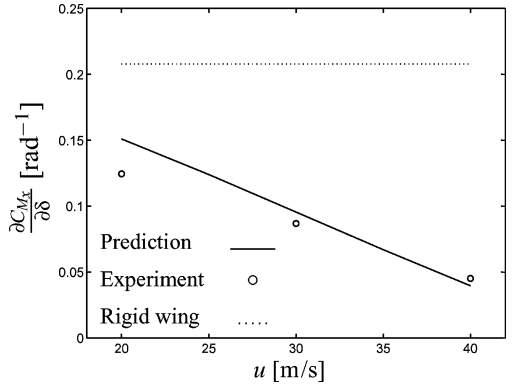

Fig. 9 Derivative of C_{M_x} with respect to δ as a function of airspeed.

The aeroelastic control surface efficiency can be expressed as

$$E_c = \left[\frac{\partial C_{M_x}}{\partial \delta}\right]_{\text{elastic}} \Bigg/ \left[\frac{\partial C_{M_x}}{\partial \delta}\right]_{\text{rigid}} \tag{3}$$

C_{M_x} is the normalized coefficient of the moment M_x around the x axis (body-fixed system) according to

$$C_{M_x} = M_x / q S_{\text{ref}} b_{\text{ref}} \tag{4}$$

where $b_{\text{ref}} = 1.350$ m denotes the reference semispan according to Fig. 1. The aerodynamic derivative of C_{M_x} with respect to the control surface deflection angle δ as a function of airspeed u is presented in Fig. 9. As shown, the aeroelastic effect on the control surface efficiency is already substantial at 20 m/s. At 40 m/s, the effect of a control surface deflection is reduced to about 20% of the corresponding effect when a rigid wing is considered. According to both the numerical and experimental results, control reversal would occur near 50 m/s. Unfortunately, no experiments are performed at that airspeed.

The resulting wing deformations are also studied for various control surface deflections. Figure 10 shows the wing deflection and elastic twist for negative and positive deflections of the control surface at $u = 30$ m/s and $\alpha = 0$ deg. Here, wing deflection refers to the out-of-plane displacement at the beam centerline, which is measured at ten spanwise positions. The wing elastic twist is also presented at the same spanwise locations. The deflection of the wing is overpredicted by approximately 15%. According to Fig. 9, the measured moment is slightly smaller than predicted at $u = 30$ m/s, and this can explain the somewhat smaller deflections. The elastic twist is also smaller than predicted. Here, the deviation is larger than for the deflection. In spite of the discrepancies in elastic twist, the agreement between numerical and experimental data in terms of the moment M_x is very good (Fig. 8). One possible reason for this is that the actual load on the control surface in the experiment is lower than predicted. Because of the somewhat stiffer wing (in torsion), the elastic twist is reduced, and therefore, the overall agreement in the efficiency of the control surface becomes good.

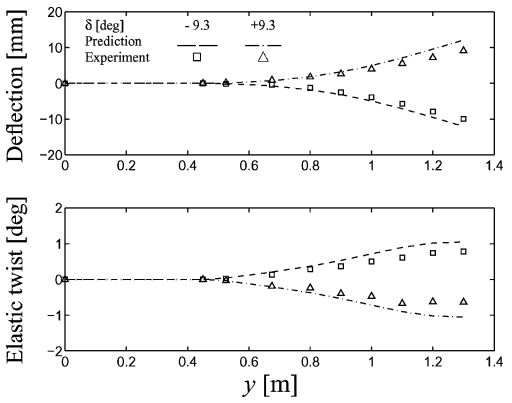

Fig. 10 Wing deformations due to control surface deflection at $u = 30$ m/s.

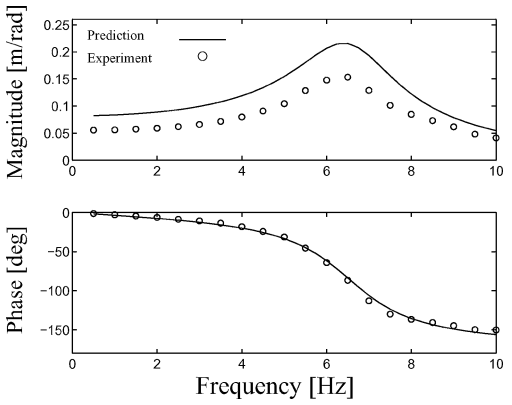

Fig. 11 Frequency response at $u = 30$ m/s.

Dynamic Response

The dynamic aeroelastic response due to sinusoidal control surface excitation is measured experimentally at various flow speeds. The two control surfaces are excited synchronously at frequencies ranging from 0.5 to 10.0 Hz. The commanded amplitude of the control surface deflection is 5 deg between 0.5 and 5.0 Hz and 3 deg in the range from 5.5 to 10.0 Hz. For accurate time control, both the control surface deflection and the wing deformation are measured using the optical system at a sampling rate of 100 Hz.

The magnitude and phase of the experimental frequency response function (FRF) between control surface deflection and wing out-of-plane deflection at the tip are shown in Fig. 11. The experimental FRF is extracted from the measured control surface deflection and wing deflection using the discrete Fourier transform.[21] The numerical analysis is performed using the aeroelastic response option in NASTRAN.

The general characteristics of the numerical FRF clearly resemble the experimental. However, the magnitude is overpredicted by the numerical model over the entire frequency range. Moreover, a resonance is observed at about 6.5 Hz. When the root-locus plot of Fig. 6 is considered, it is evident that this resonance is caused by mode A, which has a frequency in the 6-Hz range at $u = 30$ m/s. It would be interesting to investigate if a similar resonance can be found in the 20-Hz range due to mode B. However, the bandwidth of the electrical servos is not high enough for excitation at frequencies above 10 Hz.

Conclusions

The functionality of the developed design concept is proved to be good for low-speed aeroelastic investigations. In addition to the previous study,[12] it is concluded by this investigation that the elastic

wind-tunnel model can be used for studies involving control surface response. From an experimental point of view, the model in combination with the experimental setup used in this study is a versatile tool for low speed aeroelastic investigations.

Both the static and the dynamic tests indicate that the loads from the control surface are somewhat overpredicted by the numerical method. It would be interesting in future experiments to include measurements of the control surface hinge moment, or unsteady pressure distributions.

There are various possible reasons for the observed deviations. One explanation for over-estimating the control surface response could be turbulence caused by the push-rods for the control surfaces. Furthermore, no structural damping is included in the numerical analysis, and including damping may improve the numerical model when used for dynamic analysis.

Finally, the BWB concept in general provides several challenges in terms of nonconventional solutions and new ideas. Although the limitations of being a low-speed investigation, the results from this study indicate that standard type numerical tools are capable of predicting aeroelastic behavior of a BWB type of aircraft with reasonable accuracy.

Acknowledgments

This work was financially supported by the Commission of the European Union. The investigation was carried out within the project Multi-Disciplinary Design and Optimisation for Blended Wing Body Configuration with Contract G4RD-CT1999-0172. Jakob Kuttenkeuler is gratefully acknowledged for support during the investigation.

References

[1]Schweiger, J., and Krammer, J., "Active Aeroelastic Aircraft and its Impact on Structure and Flight Control System Design," Proceedings of the Applied Vehicle Technology (AVT), Paper No. 11, Fall, 1999.

[2]Weisshaar, T. A., Nam, C., and Batista-Rodrigues, A., "Aeroelastic Tailoring for Improved UAV Performance," AIAA Paper 98-1757, April 1998.

[3]Bowman, K. B., Grandhi, R. V., and Eastep, F. E. "Structural Optimization of Lifting Surfaces with Divergence and Control Reversal Constraints," *Structural Optimization*, Vol. 1, No. 3, 1989, pp. 153–161.

[4]Mantegazza, P., and Ricci, S., "Direct Approach to the Analysis of Control Reversal and its Sensitivity," *AIAA Journal*, Vol. 28, No. 11, 1990, pp. 1995–1996.

[5]Kuttenkeuler, J., and Ringertz, U. T., "Aeroelastic Tailoring Considering Uncertainties in Material Properties," *Structural Optimization*, Vol. 15, No. 3, 1998, pp. 157–162.

[6]Lind, R., and Brenner, M., *Robust Aeroservoelastic Stability Analysis*, Springer, London, 1999.

[7]Borglund, D., "Robust Aeroelastic Stability Analysis Considering Frequency-Domain Aerodynamic Uncertainty," *Journal of Aircraft*, Vol. 40, No. 1, pp. 189–193.

[8]Schneider, G., Hoenlinger, H., Guldner, W., and Manser, R., "Aeroelastic Tailoring Validation by Windtunnel Model Testing," *Proceedings of the European Forum on Aeroelasticity and Structural Dynamics*, Deutche Gesellschaft fuer Luft- und Raumfahrt, Paper No. 89-042, Bonn, Germany, 1989, pp. 399–408.

[9]Sensburg, O., Schweiger, J., Tischler, V. A., and Venkayya, V. B., "Aeroelastic Tailoring of Aerodynamic Surfaces and Low Cost Wind Tunnel Model Design," *Proceedings of the International Workshop on Multidisciplinary Design Optimization*, Rept. ADA 389797, Pretoria, South Africa, 2000, pp. 240–253.

[10]Dafnis, A., Kämpchen, M., and Reimerdes, H. G., "Aero-Structural Investigation on Highly Flexible Wind-Tunnel Models," Confederation of European Aerospace Societies/AIAA/Association de Ingenieros Aeronauticos de España International Forum on Aeroelasticity and Structural Dynamics, Paper No. 093, Vol. 111, 2001, pp. 519–531.

[11]Amiryants, G. A., and Ishmuratov, F. Z., "Multi-Purpose Modular Aerodynamic/Aeroelastic Model," *Proceedings of the CEAS/AIAA/AIAE International Forum on Aeroelasticity and Structural Dynamics*, Vol. 3, AIAE, Paper No. 092, 2001, pp. 509–518.

[12]Carlsson, M., and Kuttenkeuler, J., "Design and Testing of a Blended Wing Body Aeroelastic Wind Tunnel Model," *Journal of Aircraft*, Vol. 40, No. 1, 2003, pp. 211–213.

[13]Liebeck, R. H., Page, M. A., and Rawdon, B. K., "Blended-Wing-Body Subsonic Commercial Transport," AIAA Paper 98-0438, Jan. 1998.

[14]Cameron, D., and Princen, N., "Control Allocation Challenges and Requirements for the Blended Wing Body," AIAA Paper 2000-4339, Aug. 2000.

[15]Barlow, J. B., Rae, W. H., and Pope, A., *Low-Speed Wind Tunnel Testing*, 3rd ed., Wiley, New York, 1999, Chap. 18, pp. 687–690.

[16]Rodden, W. P., and Johnson, E. H., *MSC/NASTRAN Aeroelastic Analysis Users Guide*, Ver. 68, MacNeal–Schwendler, Los Angeles, 1994.

[17]Albano, E., and Rodden, W. P., "A Doublet-Lattice Method for Calculating Lift Distributions on Oscillating Surfaces in Subsonic Flows," *AIAA Journal*, Vol. 7, No. 2, 1969, pp. 279–285.

[18]*ProReflex Ver. 6.41, Technical Reference*, Qualisys AB, Sävedalen, Sweden, 1997.

[19]Kuttenkeuler, J., and Carlsson, M., "Optical Deformation Measurements in Wind Tunnel Testing," *Proceedings of the CEAS/AIAA/AIAE International Forum on Aeroelasticity and Structural Dynamics*, Vol. 3, AIAE Paper No. 91, 2001, pp. 499–508.

[20]Johnson, G. W., *LabVIEW Graphical Programming*, McGraw–Hill, New York, 1994.

[21]Folland, G. B., *Fourier Analysis and Its Applications*, Books/Cole Publ. Co., Pacific Grove, CA, 1992, pp. 249–255.